A quantitative approach to the cranial ontogeny of Lycalopex culpaeus *(Carnivora: Canidae)*

Valentina Segura & Francisco Prevosti

Zoomorphology
Evolutionary, Comparative and Functional Morphology

ISSN 0720-213X
Volume 131
Number 1

Zoomorphology (2012) 131:79-92
DOI 10.1007/s00435-012-0145-4

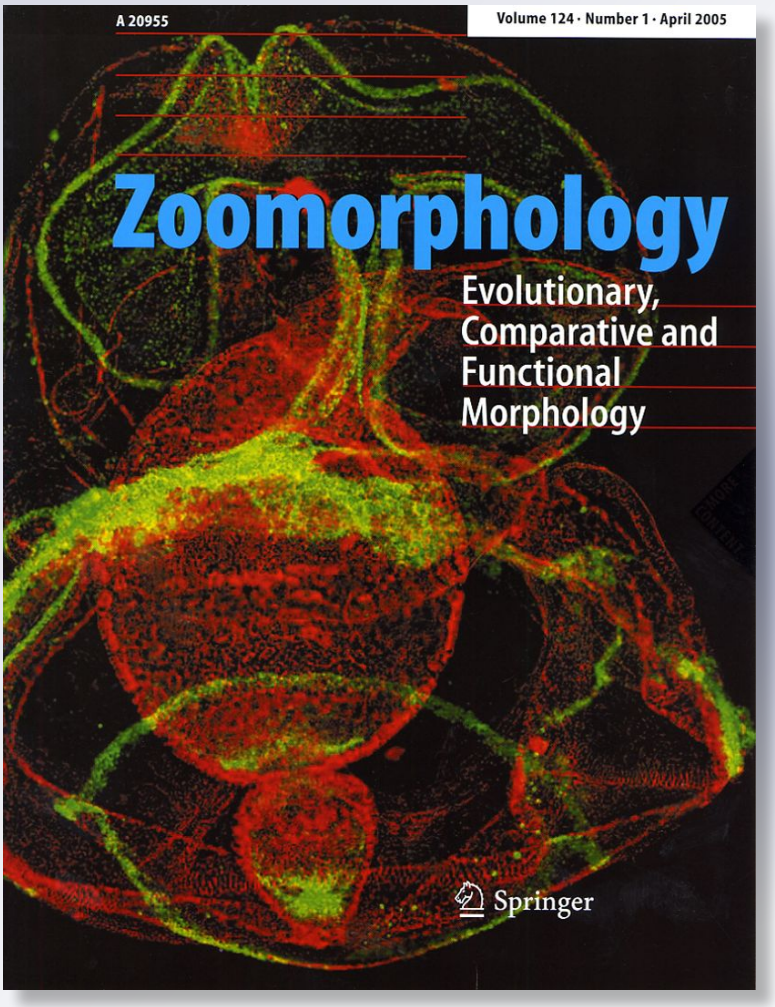

Springer

Zoomorphology (2012) 131:79–92
DOI 10.1007/s00435-012-0145-4

ORIGINAL PAPER

A quantitative approach to the cranial ontogeny of *Lycalopex culpaeus* (Carnivora: Canidae)

Valentina Segura · Francisco Prevosti

Received: 16 July 2011 / Revised: 30 December 2011 / Accepted: 2 January 2012 / Published online: 13 January 2012

Abstract The study of cranial ontogeny is important for understanding the relationship between form and function in developmental, ecological, and evolutionary contexts. The transition from lactation to the diet of adult carnivores must be accompanied by pronounced modifications in skull morphology and feeding behavior. Our goal was to study relative growth and development in the skull ontogeny of the canid *Lycalopex culpaeus*, and interpret our findings in a functional context, thereby exploring the relationship between changes in shape and size with dietary habits and age stages. We performed quantitative analyses, including multivariate allometry and geometric morphometrics. Our results indicate that shape changes are related to functional improvements of the jaw mechanics related for food catching/processing. Estimates of full muscle size, mechanical advantage, and adult cranial shape are reached after sexual maturity, while adult mandible and skull size are reached after weaning, which is related to diet change (incorporation of meat and other food items). The ontogenetic pattern observed in *L. culpaeus* is similar to those observed in *Canis familiaris* and *C. latrans*. However, the magnitude of change seen in *L. culpaeus* is smaller than those seen in the felid *Puma concolor* and considerably smaller than those seen in the bone cracker hyaenid *Crocuta crocuta.* These patterns are associated with dietary habits and specializations in skull anatomy, as *L. culpaeus*, domestic dog and coyote are generalist species compared with hypercarnivores such as *C. crocuta* and *P. concolor.*

Keywords Anatomy · Canidae · Ontogeny · Skull

Communicated by T. Bartolomaeus.

Electronic supplementary material The online version of this article (doi:10.1007/s00435-012-0145-4) contains supplementary material, which is available to authorized users.

V. Segura (✉) · F. Prevosti
División Mastozoología, Museo Argentino de Ciencias Naturales "Bernardino Rivadavia", Av. Ángel Gallardo 470, CP 1405, Ciudad Autónoma de Buenos Aires, Argentina
e-mail: vsegura@macn.gov.ar; valu_z@yahoo.com.ar

V. Segura · F. Prevosti
CONICET. Consejo Nacional de Investigaciones Científicas y Técnicas, Buenos Aires, Argentina

Introduction

The skull is a complex structure that not only houses the brain, but also the sense organs and muscles related to the opening and closing of the mandible, and to food capture and processing (Emerson and Bramble 1993; Moore 1981). Because of its complexity, the skull has been the focus of several ontogenetic studies in Mammalia, exploring how adult morphology and function are achieved (e.g., Flores et al. 2006, 2010; Giannini et al. 2004; Wayne 1986). In this context, mammalian cranial ontogeny is relevant to understand the relationship between form and function in a developmental, ecological, and evolutionary context. In carnivore species, the transition from nursing in juveniles to a carnivorous diet in adults must be accompanied by pronounced modifications in behavior and skull morphology linked to diet changes and the acquisition of new hunting methods (Binder and Van Valkenburgh 2000; Fox 1969).

Previous studies about ontogeny in canid species have focused on behavior (e.g., Bekoff 1974a, b; Biben 1982, 1983; Scott 1967), neurological responses (e.g., Fox 1964), chronology of tooth eruption and replacement (e.g., Bekoff and Jamieson 1975; Kremenak 1969; Kremenak et al. 1969;

Prevosti and Lamas 2006), and age estimation (e.g., Zapata et al. 1997). These works have presented some results in a morphological or behavioral framework, although mainly concerned with age estimation and without considering cranial characters in a functional context. Some exceptions to this are works of Wayne (1986), who studied the ontogenetic trajectories of skull growth in the domestic dog, *Canis familiaris* Linnaeus, 1758, revealing that are morphologically different than other canid species (e.g., in the latter, neonates and adults exhibit narrower palates and zygomatic breadth), and La Croix et al. (2011), who examined growth and development of skull in coyotes, *Canis latrans* Say, 1823, detecting patterns of synchronous growth and asynchronous development between skull and mandible. Drake (2011), who investigated heterochronic patterns in the skull morphology of *C. familiaris*, revealed that cranial shape of adults not resembles the cranial shape of an ontogenetic series of wolves, *Canis lupus* Linnaeus, 1758. In view of such variations, the inclusion of other canids could reveal other patterns of skull development.

Lycalopex culpaeus (Molina, 1782) is the largest representative of the genus and the second largest canid species in South America (body mass around 10 kg; Novaro 1997). These species inhabit the semidesertic Andean plateau, mediterranean scrub and grasslands, and woodland areas in western and southern South America from Colombia to southern Chile and Argentina (Novaro 1997). *L. culpaeus* has a generalist diet that includes small and medium-sized vertebrates, as well as insects and vegetables, although it is more carnivorous and consumes larger mammalian preys than other South American canid species (Jiménez and Novaro 2004; Johnson and Franklin 1994). According to its diet, *L. culpaeus* has a generalized/omnivore skull and dentition (e.g., narrow snouts and occiputs, full dentition count, well-developed grinding regions in the molar), but its dentition is more secodont (e.g., larger carnassials and cusp reductions), and its canines are longer than those of other *Lycalopex* species (Berta 1987; Kraglievich 1930; Van Valkenburgh 1988; Van Valkenburgh and Koepfli 1993).

The pioneering work of Crespo and De Carlo (1963) provided most of what is known about breeding and growth in this species. The gestation period is between 55 and 60 days, young born with eyes closed, and at 2 days of age males weigh about 166 g with a total length of 165 mm, whereas females weigh about 170 g with 161 mm of total length. The pups reach adult size in 7 months, and sexual maturity is attained during the first year. The pups nurse until weaning at 2 months of age. Post-weaning, the juveniles are still dependent while they begin to hunt with their parents until they are strong enough to feed for themselves (Crespo and De Carlo 1963; Ewer 1973). Some studies offered morphological estimators of age (e.g., Crespo and De Carlo 1963; Zapata et al. 1997) from 9 months of age, a period where mature morphology is usually reached. However, these works were unable to estimate age for earlier stages, a period defined as critical for the morphological change and the acquisition of adult characters. In this sense, the ontogenetic pattern of *L. culpaeus* has been partially studied to date, showing that quantitative analyses of cranial allometric growth and relative shape changes, emphasized in crucial ontogenetic periods, are still unknown.

In this study, we performed quantitative analyses of skull ontogeny (shape and size) of *L. culpaeus*, using multivariate allometry and geometric morphometrics. Taken together, these approaches allowed us to study the relative growth of the different cranial components. We further interpreted our findings in a functional context, exploring the relationship between size and shape changes with life history traits during the ontogeny of the largest South American fox.

Materials and methods

Sample

We analyzed an ontogenetic series of 101 skulls deposited at Museo Argentino de Ciencias Naturales Bernardino Rivadavia (MACN; see "Appendix 1"). The specimens belong to the subspecies *L. c. culpaeus* (Molina, 1782) and were captured in an ecological study performed between 1959 and 1962 in Catán Lil (39°33′S, 70°35′W), Neuquén Province, Argentina, by Crespo and De Carlo (1963). Twenty-nine specimens did not have a fully erupted dentition, whereas the remainder was comprised of animals with fully erupted dentition. Although the absolute age for both extremes of the age range (from 2 months to 11 years old) was determined by previous work (see Crespo and De Carlo 1963; Zapata et al. 1997), it is unknown for most intermediate stages. As similar studies that used age classes (e.g., La Croix et al. 2011; Tanner et al. 2010), we defined age classes in order to maximize the information for a period when major critical changes in skull morphology occur (i.e., the period from 2 months to 1 year old). Age classes were estimated from dental formulae and tooth wear, and are defined as follows:

J1, complete deciduous dentition present and with permanent P^1 and P_1 erupting;
J2, permanent I^1, I_1, and I_2 erupted and with I^2, M^1, and M_1 erupting;
J3, permanent incisors and canines erupted, with M^1 and P_2 erupted, and P^4, M^2, and M_2 erupting;
J4, definitive incisors, canines, and molars fully erupted. With P^3, P_3, P_4, and M_3 erupting;
A1, complete permanent dentition with no wear;

A2, complete permanent dentition with slight wear, with blunt cusps of incisors, canines, premolars, and molars.

A3, complete permanent dentition with dentine horns exposed on the cusps of premolars and molars and I^3 at the same level that I^1 and I^2.

Additional data are given in online resource 1

Analyses of growth and development

We test for allometric effect in skulls shape employing geometric morphometric and multivariate allometric tests for each measurement. Geometric morphometric methods test the significance of size–shape in the global configuration of the skull and multivariate allometry tests it for each measurement, thus allowing the exploration of the significance of allometry in specific skull traits. Also, geometric morphometrics are ideal to capture the shape of structures usually studied with a qualitative approach (e.g., crest development), difficult to quantify using linear measurements and the multivariate allometry approach.

For the multivariate allometry analysis, we used 25 linear measurements representing length, width, and height of skull structures in order to detect allometric trends during skull growth (Table 1; Fig. 1). This approach is based on the generalized allometry equation proposed by Jolicoeur (1963a, b). In multivariate allometry, size is regarded as a latent variable affecting all measured variables simultaneously. The elements of the first eigenvector of a principal components analysis (PCA) express the allometric relationships of all variables with the latent size. This eigenvector is extracted from a variance–covariance matrix of log-transformed variables and scaled to unity. For a given variable, allometry is the statistical deviation of its corresponding eigenvector element from a hypothetical isometric value that is expected to be equal for all elements if the global growth pattern is isometric (size invariant). The isometric element value is calculated as $1/P^{0.5}$ (0.2 for the present study) with P value equal to the number of variables. Statistical deviation from isometry was estimated using the jackknife procedure (Manly 1997; Tukey 1956) developed by Giannini et al. (2004). The purpose of this technique is to generate confidence intervals for each of the empirically derived first eigenvector elements. The confidence interval may be inclusive of the isometric (null) value 0.2 and therefore statistically indistinguishable from isometry, or it may exclude such value and therefore be considered significantly allometric: either "positive" if the observed element is >0.2 or "negative" if the observed element is <0.2. To calculate this confidence interval, n pseudosamples are generated such that a new first unit eigenvector is calculated from a matrix with one specimen of *L. culpaeus* removed at a time (with n equal to the number of specimens). In each cycle, a pseudovalue is calculated for each eigenvector element using the formula for the first-order jackknife (see Giannini et al. 2010 for details). The mean of n pseudovalues represents the jackknife estimate of the multivariate allometry coefficient for that variable. The difference between this estimate and the actual value from the complete sample is a measure of bias; we report an unbiased jackknife estimate of the allometry coefficient that results from subtracting the bias from the raw estimate (Manly 1997). The standard deviation and the corresponding 99% confidence interval (for $n - 1$ degrees of freedom) are calculated for each allometry coefficient. Giannini et al. (2004, 2010) and Flores et al. (2006) followed Manly's (1997) suggestion of using trimmed pseudovalues for the calculation of the confidence interval. Trimming the m largest and m smallest pseudovalues for each variable may significantly decrease the standard deviations and allow for more realistic allometric estimations. If untrimmed and trimmed confidence intervals greatly differ in width, this can be taken as indication of extreme pseudovalues affecting the standard errors. Here, we report both untrimmed and trimmed (with $m = 1$) calculations, opting for the results that in combination reduce bias and interval width. For the multivariate statistical analysis (PCA + jackknife resampling), an R-script (R Development Core Team 2004) from Giannini et al. (2010) was used and is available from the authors.

For the geometric morphometrics approach, we analyzed 4 views of the skull: dorsal, lateral and ventral cranium, and lateral mandible. Images of dorsal and ventral view were captured by orienting specimens with the palate parallel to the photographic plane. Images of the lateral view were obtained orienting the specimens with the sagittal plane parallel to the photographic plane. Images of lateral view of the mandible were captured orienting the long axis of the dentary parallel to the photographic plane and at the same distance from the skull. We identified and digitized, from photographs, for the skull in dorsal view 13 landmarks and 29 semi-landmarks; in ventral view, 15 landmarks and 15 semi-landmarks; in lateral view, 14 landmarks and 19 semi-landmarks, and for mandible, 7 landmarks and 15 semi-landmarks (see "Appendix 2"; Fig. 1), which could adequately describe skull shape. The landmarks used in this study were defined as type 1 and type 2, and the semi-landmarks were defined as type 3 according to Bookstein (1991). The semi-landmarks were positioned using MakeFan 6 (Sheets 2002), which draws fan-shaped lines on photographs, enabling digitization of semi-landmarks located at the intersection of the fan lines with the outlines of anatomical structures. In dorsal view, semi-landmarks were positioned at the intersection of the curving of cranial vault and zygomatic arch,

Table 1 Summary of results of multivariate cranial allometry in *L. culpaeus*

Variable	Expected allometry coefficient	Observed allometry coefficient	Observed departure	Untrimmed values				Trimmed values			
				Resampled allometry coefficient	Bias	99% CI	Growth trend	Resampled allometry coefficient	Bias	99% CI	Growth trend
CBL	0.2	0.1872	−0.0128	0.1872	−0.0008	0.1767–0.1976	−	0.1850	0.0003	0.1764–0.1936	−
HO	0.2	0.1159	−0.0841	0.1159	−0.0001	0.0954–0.1364	−	0.1161	−0.0001	0.0985–0.1337	−
MB	0.2	0.1105	−0.0895	0.1105	−0.0003	0.0942–0.1268	−	0.1109	−0.0005	0.0958–0.1259	−
BB	0.2	0.0462	−0.1538	0.0462	−0.0001	0.0224–0.0699	−	0.0511	−0.0026	0.0349–0.0672	−
BZ	0.2	0.2613	0.0613	0.2613	−0.0002	0.2343–0.2882	+	0.2677	−0.0034	0.2444–0.291	+
LO	0.2	0.1094	−0.0906	0.1094	0.0000	0.0825–0.1362	−	0.1115	−0.0011	0.0879–0.135	−
LN	0.2	0.2365	0.0365	0.2365	−0.0007	0.2130–0.2600	+	0.2376	−0.0012	0.2159–0.2592	+
LR	0.2	0.2101	0.0101	0.2101	−0.0012	0.1779–0.2423	=	0.2061	0.0008	0.1786–0.2336	=
CanB	0.2	0.1338	−0.0662	0.1338	−0.0003	0.0973–0.1704	−	0.1442	−0.0054	0.1156–0.1727	−
HM	0.2	0.1763	−0.0237	0.1763	0.0004	0.1306–0.2220	=	0.1799	−0.0014	0.1405–0.2193	=
BBu	0.2	0.0528	−0.1472	0.0528	0.0006	0.0096–0.0960	−	0.0539	0.0000	0.0152–0.0927	−
HBu	0.2	0.0078	−0.1922	0.0078	−0.0001	−0.0456–0.0612	−	0.0158	−0.0041	−0.0316–0.0633	−
LBu	0.2	0.0124	−0.1876	0.0124	−0.0002	−0.0414–0.0662	−	0.0133	−0.0007	−0.0335–0.0602	−
BP	0.2	0.0555	−0.1445	0.0555	0.0003	0.0229–0.0881	−	0.0597	−0.0019	0.0311–0.0884	−
LP	0.2	0.1800	−0.0200	0.1800	−0.0006	0.1667–0.1934	−	0.1792	−0.0002	0.1668–0.1916	−
Upr	0.2	0.2813	0.0813	0.2813	−0.0037	0.1977–0.3649	=	0.2653	0.0043	0.1881–0.3426	=
LD	0.2	0.2041	0.0041	0.2041	−0.0008	0.1942–0.2139	=	0.2028	−0.0001	0.1941–0.2115	=
HMb	0.2	0.2251	0.0251	0.2251	0.0011	0.1640–0.2863	=	0.2306	−0.0016	0.1772–0.284	=
HMr	0.2	0.2612	0.0612	0.2612	−0.0010	0.2427–0.2796	+	0.2599	−0.0003	0.2431–0.2766	+
LC	0.2	0.3132	0.1132	0.3132	0.0002	0.2536–0.3727	+	0.3251	−0.0058	0.2763–0.3739	+
Lpr	0.2	0.3353	0.1353	0.3353	−0.0039	0.2383–0.4324	+	0.3212	0.0031	0.2300–0.4125	+
Ilm	0.2	0.2382	0.0382	0.2382	0.0002	0.1920–0.2845	=	0.2401	−0.0007	0.1982–0.282	=
Ilt	0.2	0.3124	0.1124	0.3124	−0.0005	0.2831–0.3416	+	0.3125	−0.0006	0.2866–0.3384	+
Jcar	0.2	0.1655	−0.0345	0.1655	0.0003	0.1288–0.2023	=	0.1700	−0.0019	0.1358–0.2043	=
Jcan	0.2	0.2253	0.0253	0.2253	−0.0007	0.2131–0.2374	+	0.2249	−0.0005	0.2137–0.2361	+

Abbreviations as in Fig. 1 except *MB* mastoid breadth, *CanB* breadth at canines

The first three data columns show results using all specimens. The remainder of the columns shows jackknife results calculated with untrimmed and (m_1) trimmed sets of pseudovalues (see "Materials and methods"). Allometry coefficient is the correspondent element of the first (unit) eigenvector per variable. The expected coefficient (0.2) is the value under isometry (equal for all variables). The observed coefficient is the value obtained with all specimens included (n = 101). The resampled coefficient is the first-order jackknife value. Bias is the difference between the resampled and observed coefficients. The jackknife 99% confidence interval is provided; allometric variables are those whose confidence interval excludes the expected value under isometry (0.2). Growth trend is the summary allometry of each variable presented in symbols: = isometry, − negative allometry, + positive allometry

using two fans, defined by the apex of zygomatic arch, and landmarks 5, 17, and defined by supraorbital process, and landmarks 17, 25. In lateral view, were positioned at the intersection of the curving of cranial vault and muzzle, using two fans, from apex of postglenoid process, and landmarks 9, 24, apex of infraorbital process, and landmarks 18, 21, and one grid defined by landmarks 1 and 4. In ventral view, were positioned at the intersection of zygomatic arch and muzzle, using one fan, defined by apex of zygomatic arch, and landmarks 8 and 30. In mandible view, were positioned at the intersection of the curving as evenly spaced points, from landmark 1 to 10 (Fig. 1). We used tpsUtil 1.40 (Rohlf 2008a, b) to compile image files, and both landmarks and semi-landmarks were digitized onto the images using tpsDig 2.12 (Rohlf 2008a, b). TpsUtil 1.40 was also used to define "slider-files" to distinguish between real landmarks and semi-landmarks. Landmark configurations were superimposed through generalized procrustes analysis (GPA Goodall 1991; Rohlf 1999), which minimizes the sum of squared distances between homologous landmarks by translating, rotating, reflecting, and scaling them to unit (the consensus), using tpsRelw 1.35 (Rohlf 2003a, b). The centroid size, defined as the square root of the sum of squared distances of each landmark from the centroid of the landmark configuration, was used as estimate of skull and mandible size (Bookstein 1991; Zelditch et al. 2004). The procrustes coordinates of landmarks of aligned specimens were obtained with the GPA. For sliding semi-landmarks, we used the minimum bending energy of the thin plate spline function (Bookstein 1997). To better describe shape variation at different scales, we used partial warps (=PW) and uniform components (=Uni) extracted by the

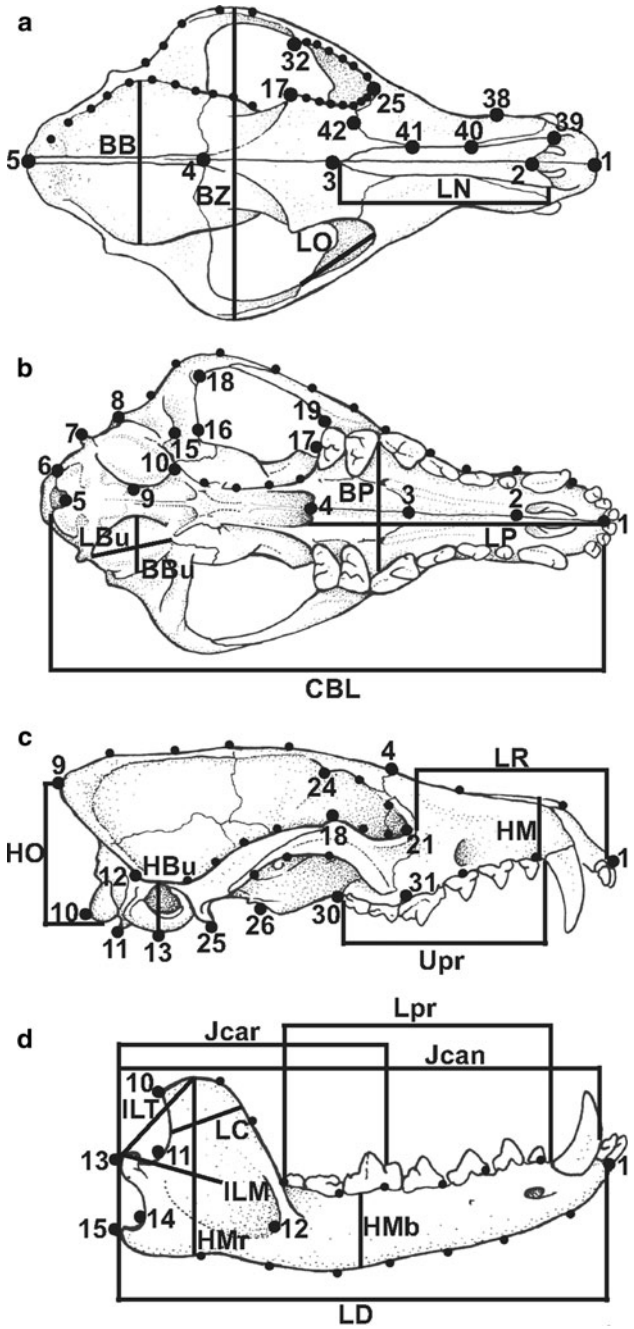

Fig. 1 Cranial landmarks (*large dots*), semi-landmarks (*small dots*), and measurements of *Lycalopex culpaeus* for dorsal (**a**), ventral (**b**), lateral (**c**), and mandible (**d**) views. *BB* breadth of braincase, *BBu* breadth of auditory bulla, *BP* breadth of palate, *BZ* interzygomatic breadth, *CBL* condylobasal length, *HBu* height of auditory bulla, *HM* height of muzzle, *HMb* height of mandibular body, *HMr* height of mandibular ramus, *HO* height of occipital plate, *Ilm* in-lever of the masseter, *Ilt* in-lever of the temporalis, *Jcan* out-lever to canine point, *Jcar* out-lever to carnassial point, *LBu* length of auditory bulla, *LC* length of coronoid process, *LD* length of mandible, *LN* length of nasals, *LO* length of orbit, *LP* length of palate, *Lpr* length of lower postcanine row, *LR* length of rostrum, *Upr* length of upper postcanine row

bending energy matrix of the thin plate spline function. An allometric analysis was performed by regressing the partial warps (and the uniform components) of the complete pooled sample, calculated from the coordinates obtained from the GPA, on the centroid size (with the tpsRegr 1.28 software; Rohlf 2003a, b). The change of shape along the size (centroid size) gradient was illustrated through deformation grids obtained with tpsRegr 1.28. The significance of the regression was tested with the Generalized Goodall *F* test, the Wilks' Lambda, and a permutation test with 1,000 resamples. Procrustes distance between each specimen and the consensus of the youngest category was used as an index of shape change (see Tanner et al. 2010) and was calculated as the square root of the summation of the distance between each landmark of 1 specimen and this mean. These estimations were calculated with the software R 2.9.2 (R Development Core Team 2004). Differences in size, shape (procrustes distance), and mechanical advantage of masseter and temporal muscles between successive age classes were tested with the Mann–Whitney *U* test (Zar 1984).

Previous authors showed that *L. culpaeus* presents some sexual dimorphism in adult external and cranial measurements (Crespo and De Carlo 1963; Johnson and Franklin 1994; Travaini et al. 2000). In this sense, we tested the presence of sexual dimorphism in size (centroid size) and shape (landmark coordinates of aligned specimens obtained in the GPA) using the Mann–Whitney *U* test (Zar 1984) and the nonparametric MANOVA (Anderson 2001), respectively. These analyses were performed with the software PAST 1.98 (Hammer et al. 2001). The distribution of females, males, and unsexed specimens in the age classes was: J1: 2/3/2; J2: 2/1/0, J3: 1/2/2; J4: 5/5/4, A1: 13/13/4; A2: 13/13/0; A3: 3/4/9. Unfortunately, for most of the juvenile classes, the proportion of sexed specimens was very low. Due to this, and to the general absence of significant sexual dimorphism in size and shape (only shape of the skull in lateral view of class A1, centroid size of all views of class A2, centroid size of mandible, ventral and lateral skull views of class A3 were significant with $P \leq 0.05$), we pooled the sexes together in each age class. The allometric analyses of male and female subsamples gave the same pattern of ontogenetic variation, in relation to each other and to the whole sample analysis (data not showed). They indicate that the observed allometric pattern is not biased by the sexual dimorphism present in size; thus, we were confident to pool the whole sample.

Mechanical advantage

We calculated the mechanical advantage and size of the temporalis and masseter masticatory muscles in order to infer relative bite force, following Radinsky (1981) and

Tanner et al. (2010). Mechanical advantage was estimated as the in-lever of each muscle divided by out-lever for each muscle. The in-lever of the temporalis was measured as the distance from the dorsal tip of the coronoid process to the mandibular condyle (Ilt) and the in-lever of the masseter as the distance from the mandibular condyle to the middle of the masseteric fossa (Ilm). Out-levers for both muscles were measured as the distance from the mandibular condyle to the bite point (in this work, to the carnassial notch, Jcar, and to the center of the crown of lower canine, Jcan). Masticatory muscle size was also estimated as the maximum width across the zygomatic arches BZ (Fig. 1).

Results

Multivariate allometry

The first principal component accounts for 70.8% of the total variance. Observed multivariate coefficients of allometry varied widely across variables (Table 1; Fig. 1). Average estimated bias (using absolute jackknife values) across coefficients calculated from trimmed and untrimmed values were both small (0.0007 and 0.0017, respectively). Trend obtained with untrimmed and trimmed values did not differ in any of the variables, that is, extreme pseudovalues did not affect jackknife estimates. Two variables showed the smallest observed departure from isometry: length of the mandible (LD) and length of the rostrum (LR), (0.0041 and 0.0101, respectively, Table 1), which could be considered as independent variables in further bivariate analyses of allometry. Height of the bulla exhibited the largest departure from isometry (−0.1922). Eighteen variables significantly departed from isometry, 11 of them were negatively allometric mostly related with the neurocranium: breadth of braincase (BB), length of orbit (LO), height of occipital plate (HO), intermastoid breadth (MB), height of auditory bulla (HBu), length of auditory bulla (LBu), breadth of auditory bulla (BBu), breadth of palate (BP), length of palate (LP), condylobasal length (CBL), and intercanine breadth (CanB). Seven of them were positively allometric and related with the splachnocranium: jaw joint to canines (Jcan), height of mandibular ramus (HMr), length of coronoid process (LC), length of lower postcanine row (Lpr), in-lever of temporalis muscle (Ilt), zygomatic breadth (BZ), and length of nasals (LN).

Geometric morphometrics

In the analysis of dorsal view, size explained 5.2727% of the shape, a relationship that was highly significant ($F = 5.4096$, $P < 0.0001$, Wilks' Lambda = 0.1778). Juvenile specimens showed a relatively smaller temporal fossa, a thinner zygomatic arch, a wider postorbital constriction, a supraorbital process with smoother outline, a rounder braincase and a wider and shorter muzzle (Fig. 2a). Adult specimens were characterized by relatively elongated nasals, a larger temporal fossa, more developed zygomatic arches, a narrower postorbital constriction and braincase (Fig. 2a).

In the analysis of the ventral view, size significantly explained 7.9055% of shape ($F = 8.2500$, $P < 0.0001$, Wilks' Lambda = 0.1585). Juvenile skulls were associated with a relatively narrower zygomatic arch and shorter broader muzzle (Fig. 2b). Adult skulls were associated with relatively stronger, wider zygomatic arches, wider temporal fossae, relatively closed glenoid fossae, and shorter palatines (Fig. 2b).

In the analysis of the lateral view of the skull, size explained 3.3765% of the shape ($F = 3.3978$, $P < 0.0001$, Wilks' Lambda = 0.1375). Juvenile skulls had a relatively rounded braincase, short rostrum, and the zygomatic arch and orbit in a lower and more lateral position (Fig. 2c). Adult skulls were associated with a relative growth of the infraorbital process, change of position in the orbit from lateral to latero-dorsal, flattening of the braincase and occipital plate, strengthening of the zygomatic arch and its shift to a more latero-dorsal position, lengthening of the upper postcanine row, and muzzle elongation (Fig. 2c).

In the mandible analysis, size explained 5.8779% of the shape variation ($F = 6.1871$, $P < 0.0001$, Wilks' Lambda = 0.1757). Juvenile skulls were associated with a relatively thinner and more curved mandibular corpus, and a thinner mandibular ramus more posteriorly placed (Fig. 2d). Adult skulls were associated with a relatively more elongated masseteric fossa, more developed angular process, greater separation between condyloid and angular processes, straighter mandibular body, a more vertical coronoid process and thicker mandibular ramus (Fig. 2d).

Changes in size, shape, and mechanical advantages throughout ontogeny

Median skull size, measured as centroid size of each view of the crania and mandible (Figs. 3a, b), showed rapid and sustained growth from age class J1 to J2/J3 when the adult size is reached. We only found significant differences between classes J1–J2 with the Mann–Whitney *U* test (See Table 2).

The median shape change index of dorsal (Fig. 3c) and ventral views showed similar values for juvenile classes, then increased beginning in class A1, and next decreased in the last class A3 in the ventral view. Lateral skull and mandible (Fig. 3d) views showed a sustained growth from J1 to J4 and then shape reached an asymptote from J4 to A3. These tendencies were based on median values for each category, but there was a large amount of variation that

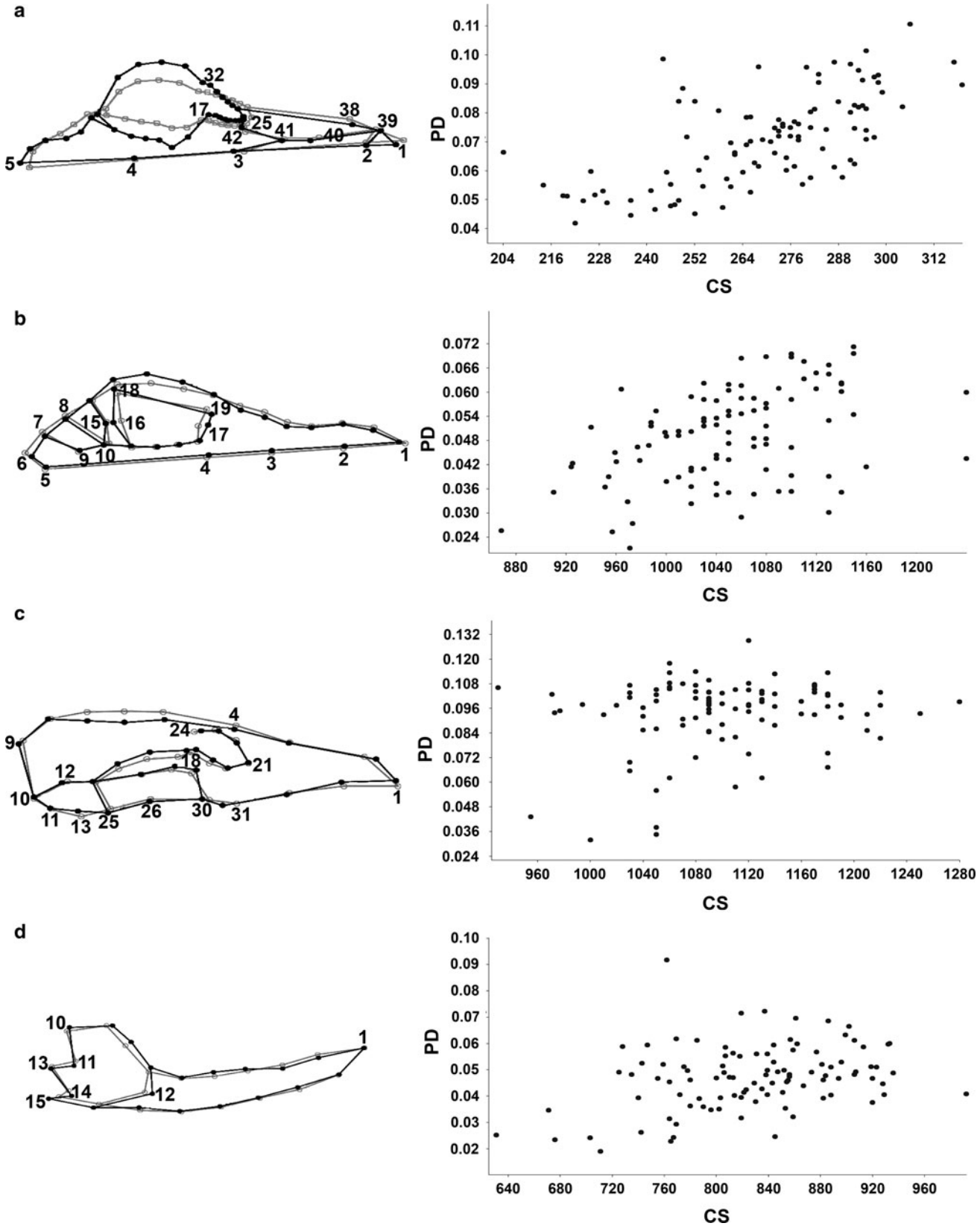

Fig. 2 Allometric change of the skull and biplots of centroid size (*CS*) versus procrustes distance (*PD*) of *Lycalopex culpaeus*, for dorsal (**a**), ventral (**b**), lateral (**c**), and mandible (**d**) views. For each view, the lower size extreme (*light color*) and upper extreme of size (*dark color*)

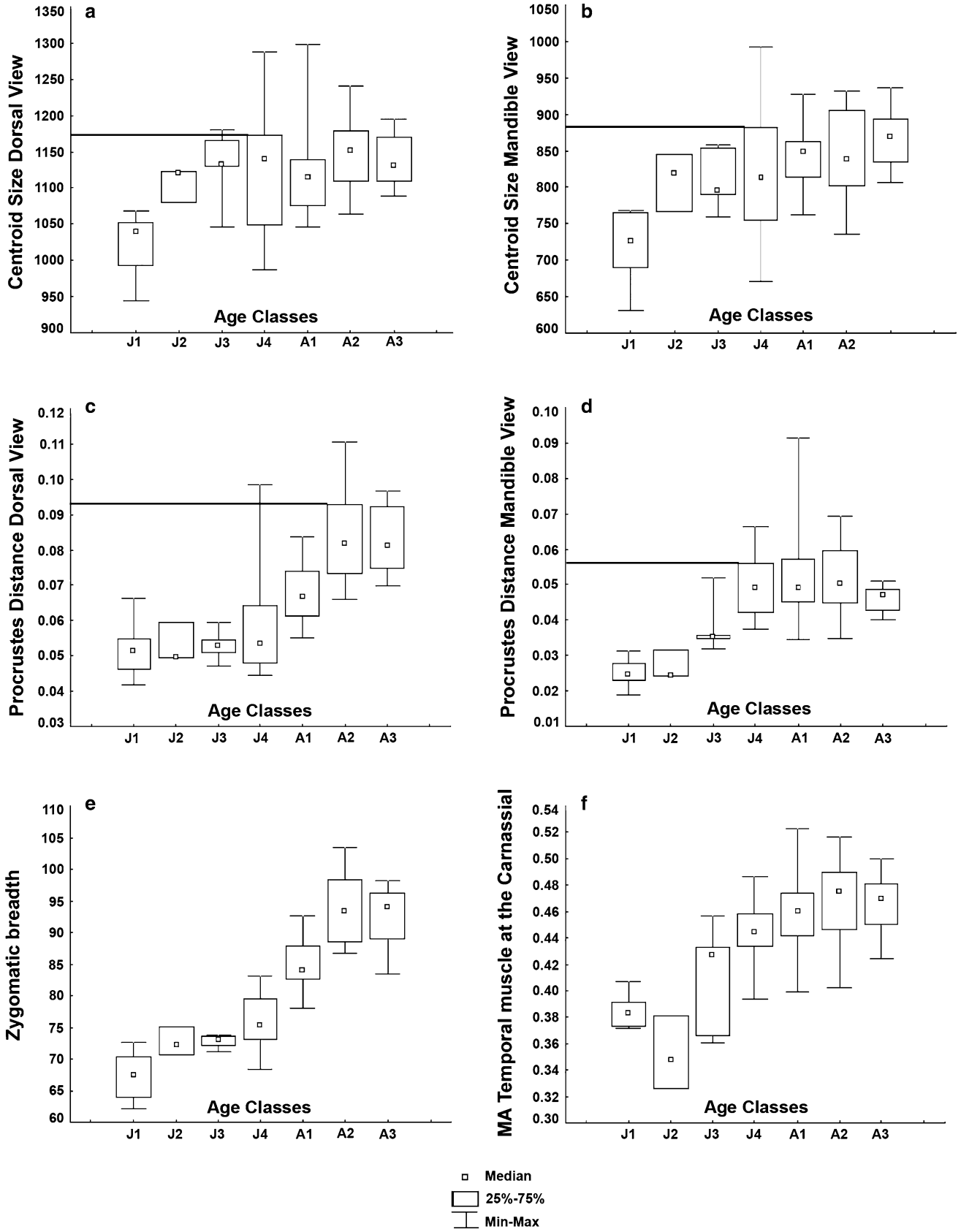

◀ **Fig. 3** *Boxplots* of skull centroid size versus age classes of *Lycalopex culpaeus*, for dorsal (**a**) and mandible (**b**) views. *Boxplots* of skull procrustes distance of each specimen of all age classes to the mean of J1 class, for dorsal (**c**) and mandible (**d**) views. *Boxplots* of mechanical advantage (*MA*) versus age classes of zygomatic breadth (**e**) and mechanical advantage of temporal muscle measure at the carnassial (**f**). The *boxplots* include median, upper, and lower quartiles (75 and 25%, respectively), minimum and maximum. In **a** and **b,** *horizontal lines* indicate the offset of development in shape and in **c** and **d** growth in size

Table 2 Summary of results of Mann–Whitney *U* test for cranial allometry in *L. culpaeus*

	U	*n*1	*n*2	*P*
J1–J2 dorsal view	0	7	3	<0.0170
J1–J2 ventral view	0	7	3	<0.0170
J1–J2 lateral view	0	7	3	<0.0170
J1–J2 mandible view	1	8	3	<0.0250
J2–J3 mandible view	0	3	5	<0.0260
J3–J4 lateral view	7	5	14	<0.0096
J3–J4 mandible view	7	5	14	<0.0096
J4–A1 dorsal view	90	23	21	<0.0004
J4–A1 ventral view	57	14	30	<0.0002
A1–A2 dorsal view	97	21	26	<0.0002
A1–A2 ventral view	89	30	25	<0.0001
Zygomatic breadth	57	14	31	<0.0001
Temporal mechanical advantages J4–A1 at canine	110	14	31	<0.0090
Temporal mechanical advantages J4–A1 at carnassial	133	14	31	<0.0400
Temporal mechanical advantages A1–A2 at canine	76.5	31	23	<0.0001

became evident in the overlap of the ranges as well as in the 25 and 75% quartiles (Figs. 3c, d). Mann–Whitney *U* test only detected significant differences between classes J4–A1 and A1–A2 in dorsal (See Table 2).

There were clear patterns of ontogenetic change in the mechanical advantage of the masseter and temporalis muscles. Median BZ showed a sharp increase from class J1 to A2–A3 (Fig. 3e). The mechanical advantage of the masseter muscle measured at the canine showed a pattern of slight decrease with higher values for class J1 decreasing toward J4, but these differences were small and the trend was not very clear. Median mechanical advantage of the masseter measured at the carnassial showed a slight increase until class A1 when it reached adult values. The median mechanical advantage of the temporal muscle measured at the canine and carnassial showed a sustained increase from J2 to A2 and a slight decline in value for class A3 (Fig. 3f). The J2 class possessed the lowest median in some of these measurements. The only significant differences detected by the Mann–Whitney *U* test were the BZ (See Table 2). Additional data are given in online resource 2, 3, and 4.

Discussion

Postnatal skull ontogeny in *Lycalopex culpaeus*

Morphologic and morphometric transformations and interactions between the neurocranium and splachnocranium have profound impacts on the strength and function of the adult skull. The detected changes encompassed the relative enlargement of the temporal fossa (related with positive allometry of zygomatic breadth, BZ, and negative allometry of braincase, BB) and a relative decrease in size of the postorbital constriction, occipital plate (HO and MB), and the braincase (BB). Sensory capsules such as auditory bulla (BBu, HBu, and LBu) and LO, also scaled negatively following the general pattern of most vertebrates (e.g., Emerson and Bramble 1993; Table 1). The splanchnocranium underwent growth and strengthening that affected the BZ, deepening of the masseteric fossa, and reaching a vertical orientation of the coronoid process (Fig. 2). The observed positive allometry of most mandibular variables and the in-lever of temporalis (Ilt, Table 1) is related to an increase in bite force and stress support during prey apprehension as acquired in other carnivorans (Slater et al. 2009; Tseng 2009; Tseng and Wang 2010; see below). The palate being relatively longer and wider in young *L. culpaeus*, developed by the negative allometry in its length (LP), breadth (BP), and intercanine breadth (CanB, Table 1). These features are associated with a functional condition of the palate in young, which acts as a platform of the tongue during suckling, as observed in some marsupial carnivores (e.g., *Didelphis albiventris* Lund, 1840, Abdala et al. 2001; *Dasyurus albopunctatus* Schlegel, 1880, Flores et al. 2006). On the other hand, the rostrum of *L. culpaeus* showed a different pattern with positive allometry in nasals (LN) and isometry in upper postcanine row (Upr, Table 1). Such complexity of the splanchnocranium can also be detected in different allometric trends obtained for both postcanine rows, isometric in the upper (Upr), and positively allometric in the lower one (Lpr), while both postcanine rows are of the same length in adults. This can be related with the dental eruption sequence in *L. culpaeus*. Normally, the upper postcanine row has 1 more tooth than the lower row at a given time, until the final tooth count is attained in adults (see age classes description). Therefore, this difference is compensated by a faster rate of growth to maintain the same length in the upper and lower tooth row. The lower tooth row, having started with fewer teeth, grows faster to reach its final length. An inverse pattern of growth was detected in some didelphids (Abdala et al. 2001, Flores et al. 2003).

In relation to the cranial shape change along the ontogenetic sequence (Figs. 3c, d), we observed that the dorsal and ventral views reach the adult shape at class A2. This class includes specimens being more than 1 year old and sexually mature (Novaro 1997). The lateral and mandibular views reached adult shape earlier, at the J4 age class, including young specimens with not yet fully erupted permanent dentition, but with adult size. This is in agreement with Crespo and De Carlo (1963), who reported that juveniles at 7 months of age are similar to adults in general appearance and body size (about 10 kg). This was also confirmed by the plot of centroid size by age categories (Fig. 3a, b) where the size of each cranial and mandible views reached adult figures in J4 class, although also we detected large variation in the sample of this class. In any case, it must be noted that the median of the earlier classes (i.e., J3 or even J2) had similar values to the older ones, indicating that size changes happened earlier, before reaching adult shape, which happens between J4 and A2.

Zygomatic arch breadth, which reflects the size of jaw musculature, is allometrically positive (Table 1), increased rapidly, and showed stable values in age class A2, but with slight decrease in A3 (Fig. 3e). This might be the result of bone resorption and muscle weakness that occurs in very old specimens (>10 years old; Jiménez and Novaro 2004). The abrupt progression of this measure is followed by other estimators of mechanical advantage. In some cases, mechanical advantage of the temporalis at the carnassial and at the canine increases through ontogeny, except when going from J1 to J2. This fact might have been an error generated by the low sample size and the large variation represented by this class (Fig. 3f). The mechanical advantage of the temporalis at the carnassial increased more progressively than those measured at the canine, while in the case of the masseteric, the increase in mechanical advantage at the carnassial was less marked (Fig. 3f). Values of the masseteric mechanical advantage were highly variable throughout ontogeny, although similar to the advantage at the carnassial and the canine, with a slight decrease in the latter and a stronger advantage at the carnassial, as observed in the A1 to A3 classes. The detected pattern of change in the mechanical advantages was similar to the observed in shape changes (Fig. 3c–f), but contrasting with the changes in centroid size along the ontogeny of *L. culpaeus* (Fig. 3a, b).

Ontogeny and feeding performance

These ontogenetic changes paralleled the acquisition of an omnivorous diet (although includes insects and vegetables, also includes hunting and processing of vertebrates preys) and affected mainly the trophic apparatus, the occiput and, presumably, their linked functions (feeding and head movements). Such characters are linked with larger volume of the masticatory muscles and their insertion areas, as well as with the amount of mechanical resistance of the food and preys. The interaction of morphologic and morphometric changes of the neurocranium and trophic apparatus described herein was expected, because growth pattern in *L. culpaeus* coincides with changes in feeding habits (from lactation to omnivorous diet) and the learning of hunting and killing prey methods required for an independent existence as a predator (Binder and Van Valkenburgh 2000; Ewer 1973). Shape changes (Fig. 2) and allometric growth trends (Table 1) are clearly related to functional improvements in terms of jaw mechanics, prey capture, and food ingestion and processing, as most of the definitive jaw muscle size and advantage, as well as the adult cranial shape (except for the mandible and lateral view of the skull) are reached after sexual maturity (around 1 year) at age category A2. The age of maturity is probably related to the time of independence and dispersion of individuals (Ewer 1973) when a more efficient skull and mandibular complex are needed to hunt and process prey. The delay between sexual maturity and the attainment of adult cranial morphology indicates that *L. culpaeus* have an "adjustment" period when they do not yet possess full adult levels of feeding performance, as observed in other species (e.g., Tanner et al. 2010; see below). In contrast, adult mandible and skull size are reached after weaning (≈2 months, see Crespo and De Carlo 1963; Novaro 1997), in class J2, just when the diet changes by the incorporation of meat and other food items occur.

Comparison with other species of the Carnivora

Both limited information and lack of knowledge about cranial ontogeny in other terrestrial carnivores restricted the comparison of the cranial ontogenetic pattern described for *L. culpaeus*. However, some information about allometric trends based on skull measurements and qualitative description is available for domestic dogs, *C. familiaris* and cougars, *Puma concolor* (Linnaeus, 1771) (Evans 1993; Gay and Best 1996; Giannini et al. 2010; Segura and Flores 2009; Wayne 1986), and geometric morphometric analyses have been recently conducted for the spotted hyaena, *Crocuta crocuta* (Erxleben, 1777) (Tanner et al. 2010), coyotes, *C. latrans* (La Croix et al. 2011) and for dogs, *C. familiaris* and wolves, *C. lupus* (Drake 2011).

Compared with *C. familiaris*, *L. culpaeus* does not share the same scaling pattern in skull length (here negatively allometric) but shares the allometric scaling pattern of skull width and depth, which results in dramatic changes in the relative skull width of puppies as they grow (Wayne 1986). However, the results of Wayne (1986) were based on a mesaticephalic dog breed (German shepherds, with average skull), whereas nothing is known about the ontogenetic

arrangement in morphologically extreme breeds (doliocephalic and brachycephalic). Puppies with short and wide skulls as observed in *L. culpaeus* (Fig. 2) seem to be a generalized characteristic in canids, because it is a pattern also detected in *C. familiaris* (Wayne, 1986), *C. latrans* (La Croix et al. 2011), and *C. lupus* (Drake 2011). Additionally, some *C. familiaris* breeds (adult specimens) exhibit a characteristic rearrangement of the skull in which the palate and basicranium rotate each other (Drake 2011). *L. culpaeus* does not share these adjustments with these dogs but *C. lupus*, in which palate and basicranium remain in the same plane throughout development. Other canids such as *C. latrans* present a similar pattern in the growth of its sagittal and occipital crests, angular and coronoid processes, and narrowing of the braincase, but not in strong elongation of the rostrum and narrowing of the zygomatic arches (La Croix et al. 2011). These differences could be partly due to the lack of very young specimens in our sample (i.e., neonates and pre-weaning) that have extremely short rostrum. *C. latrans* reach their adult mandible and skull size before sexual maturation, as in *L. culpaeus* (La Croix et al. 2011), but its adult skull shape is attained even earlier than adult size, and only the adult shape of the mandible is reached after adult size. This is a sharp difference with *L. culpaeus*, in which the final adult skull shape in ventral and dorsal views is reached after sexual maturation.

Although *L. culpaeus* and the felid *P. concolor* probably show greater ontogenetic differences in the orbitotemporal and mandible regions in strictly morphological terms (see Segura and Flores 2009), both species exhibited a similar pattern of allometric growth, with negative trends in sensory capsules (orbit, tympanic bulla, and breadth of braincase among others) and positive allometry variables related with the trophic apparatus such as zygomatic breadth, height of mandibular ramus, length of coronoid process, suggesting that the sensory capsules grow at a slower pace than the splachnocranium (see Giannini et al. 2010). Negative allometry of the braincase and sensory capsules through ontogeny is a general pattern that has also been observed in other carnivorous or omnivorous metatherian mammals such as *D. albopunctatus*, *Lutreolina crassicaudata* (Desmarest, 1804), *D. albiventris,* and *Caluromys philander* (Linnaeus, 1758) (Abdala et al. 2001; Flores et al. 2003, 2006, 2010) and could be linked to the retention of a plesiomorphic feature. Indeed, negative allometry of some sensory capsules (e.g., orbits) was detected in static interspecific allometric studies (Finarelli and Goswami 2009; Noble et al. 2000; Ravosa et al. 2000) made only on adult specimens, which was related to encephalization and orbit orientation.

The ontogenetic change observed in *C. crocuta* also showed the same tendency of strengthening of the skull associated with weaning and shifting to a carnivorous diet, as observed in *P. concolor* (Giannini et al. 2010; Segura and Flores 2009) and *L. culpaeus* (this report). However, although the skulls of the juveniles of both species were similar in shape, adult hyenas had more remarkable morphological change than adult *L. culpaeus* (see Tanner et al. 2010, Figs. 4, 5, 6, 7), probably related to a more specialized diet and bone processing (Biknevicius and Leigh 1997; Binder and Van Valkenburgh 2000). An additional difference is that in *L. culpaeus*, adult skull size was reached before sexual maturity, but adult shape for most cranial views and muscle advantage (bite forces) values were reached after this age, with the exception of the lateral view of the skull and the mandible, which attain adult configurations in subadult age (class J4, around 7 months). In contrast, adult skull size in *Crocuta* was reached soon after reproductive maturity and adult shape, a year after that (Tanner et al. 2010).

Conclusion

In summary, the ontogenetic pattern observed in *L. culpaeus* was similar to that of its close relatives, *C. familiaris* and *C. latrans* (Wayne 1986; La Croix et al. 2011), but presented less morphological changes compared to that of the hyaenid *C. crocuta* (Tanner et al. 2010). The felid *P. concolor* possessed an intermediate pattern, with strong changes (see Tables 1 and 2 in Segura and Flores 2009), and more profound shape changes than those of the *L. culpaeus*, but less than those observed in *Crocuta* (see Fig. 1 in Tanner et al. 2010). Such diverse patterns are linked to dietary habits and specialization that impact skull anatomy (Van Valkenburgh 1989, 2007), because both the *L. culpaeus* and the domestic dog are generalized species (Novaro 1997), while *P. concolor* and *C. crocuta* are hypercarnivores (Holekamp and Kolowski 2009), the latter also being ossiphagous (Tseng and Binder 2010). If this hypothesis is correct, we would expect more changes (e.g., more development of nuchal and sagittal crests, strengthening of zygomatic arch and mandible, and decreasing of breadth of braincase) in postnatal skull morphology in more specialized taxa. On the other hand, *P. concolor* and *Crocuta* have a more recent common ancestor in comparison with the other studied carnivores, while the canids belong to the same clade (Canidae); thus, it is possible that the pattern of similarities/differences observed between the skull ontogeny of these carnivores could be explained by phylogenetical relatedness. More carnivorous species must be analyzed to test these hypotheses and to evaluate the potential presence of a phylogenetic pattern in the cranial ontogeny of these carnivores.

Acknowledgments We thank David Flores for the permission to study the material under his care; to Pablo Teta for his drawings of *L. culpaeus* skulls; to Erika Hingst-Zaher, Amelia Chemisquy, and David Flores for their critical revision of the preliminary version of this manuscript and to Cecilia Morgan for her revision of English grammar. We also thank to three anonymous reviewers who provided many helpful suggestions to this study. This research was partially supported by CONICET (PIP 01054) and ANPCyT (PICT 2008-1798).

Appendix 1

Specimens of *Lycalopex culpaeus* of Museo Argentino de Ciencias Naturales Bernardino Rivadavia (MACN) used in this study

15022; 15024; 15025; 15028; 15033; 15037; 15040; 15044; 15045; 15049; 15050;15055; 15062; 15063; 15064; 15073; 15078; 15081; 15082; 15083; 15089; 15093; 15096; 15101; 15106; 15112; 15119; 15121; 15122; 15123; 15124; 15127; 15129; 15130; 15131; 15132; 15133; 15138; 15140; 15149; 15151; 15154; 15158; 15163; 15168; 15172; 15173; 15177; 15180; 15181; 15182; 15190; 15194; 15196; 15197; 15199; 15200; 15201; 15202; 15203; 15208; 15212; 15220; 15223; 15224; 15226; 15227; 15228; 15229; 15232; 15233; 15240; 15243; 15246; 15248; 15258; 15259; 15260; 15261; 15266; 15267; 15268; 23072; 23076; 23077; 23093; 23095; 23098; 23099; 23100; 23101; 23102; 23103; 23104; 23108; 23119; 23123; 23125; 23143; 23148; 23152.

Appendix 2

Definition of the landmarks and semi-landmarks used in the geometric morphometric analyses (see Fig. 1)

Dorsal landmarks: 1, tip of premaxilla in the sutura interincisiva; 2, anterior portion of the nasals in the sutura internasalis; 3, midline of sutura frontonasalis; 4, intersection between sutura coronalis, sutura sagittalis, and sutura interfrontalis; 5, tip of occipital plate; 6–16, semi-landmarks; 17, tip of the supraorbital process; 18–24, semi-landmarks; 25, lacrimal foramen; 26–31, semi-landmarks; 32, tip of the infraorbital process; 33–37, semi-landmarks; 38, apex of canine root; 39, nasal process; 40, anterior contact of sutura nasomaxillaris; 41, posterior contact of sutura nasomaxillaris; 42, apex of sutura frontomaxillaris.

Ventral landmarks: 1, anterior tip of premaxilla; 2, midline in Sutura incisivomaxillaris; 3, midline in Sutura palatomaxillaris; 4, posterior point of palatine torus; 5, anterior point of intercondyloid incisure; 6, internal apex of occipital condyle; 7, apex of jugular process. 8, tip of mastoid process; 9, internal apex of tympanic bulla; 10, anterior apex of tympanic bulla; 11–14, semi-landmarks; 15, tip of postglenoid process; 16, internal edge of masseteric fossa; 17, caudal apex of border of palatine; 18, external edge of masseteric fossa; 19, anterior edge of masseteric fossa; 20–30, semi-landmarks.

Lateral landmarks: 1, tip of premaxilla; 2–3, semi-landmarks; 4, apex of sutura frontomaxillaris; 5–8, semi-landmarks; 9, posterior point between sagittal and nuchal crests; 10, apex of occipital condyle; 11, tip of paracondylar process; 12, point between nuchal crest and mastoid process; 13, apex of tympanic bulla; 14–17, semi-landmarks; 18, tip of infraorbital process; 19–20, semi-landmarks; 21, lacrimal foramen; 22–23, semi-landmarks; 24, tip of the supraorbital process; 25, tip of Postglenoid process; 26, posterior point of pterygoid; 27–29, semi-landmarks; 30, posterior tip of dentary row; 31, notch of carnassial; and 32–33, semi-landmarks.

Mandibular landmarks: 1, anterior tip of body of mandible; 2–9, semi-landmarks; 10, posterior tip of coronoid process; 11, mandibular notch; 12, anterior point of masseteric fossa; 13, external point of condyloid process; 14, separation between condyloid and angular process; 15, tip of angular process; 16–22, semi-landmarks.

References

Abdala F, Flores DA, Giannini NP (2001) Postweaning ontogeny in the skull in *Didelphis albiventris*. J Mamm 82:190–200

Anderson MJ (2001) A new method for non-parametric multivariate analysis of variance. Aust Ecol 26:32–46

Bekoff M (1974a) Social play in coyotes, wolves, and dogs. Bioscience 24:225–230

Bekoff M (1974b) Social play and play-soliciting by infant canids. Am Zool 14:323–340

Bekoff M, Jamieson R (1975) Physical development in coyotes (*Canis latrans*), with a comparison to other canids. J Mamm 56:685–692

Berta A (1987) Origin, diversification, and zoogeography of the south American Canidae. Fieldiana Zool 39:455–471

Biben M (1982) Object play and social treatment of prey in bush dogs and crab-eating foxes. Behaviour 79:201–211

Biben M (1983) Comparative ontogeny of social behaviour in three South American canids, the maned wolf, crab-eating fox and bush dog: implications for sociality. Ani Behav 31:814–826

Biknevicius AR, Leigh SR (1997) Patterns of growth of the mandibular corpus in spotted hyenas (*Crocuta crocuta*) and cougars (*Puma concolor*). Zool J Linn Soc 120:139–161

Binder WJ, Van Valkenburgh B (2000) Development of bite strength and feeding behavior in juvenile spotted hyenas (*Crocuta crocuta*). J Zool 252:273–283

Bookstein FL (1991) Morphometric tools for landmark data. Geometry and biology. Cambridge University Press, USA

Bookstein FL (1997) Landmark methods for forms without landmarks: morphometrics of group differences in outline shape. Med Image Anal 1:225–243

Crespo JA, De Carlo JM (1963) Estudio ecológico de una población de zorros colorados *Dusicyon culpaeus*. Rev Mus Argent Cienc Nat 1:1–55

Drake AG (2011) Dispelling dog dogma: an investigation of heterochrony in dogs using 3D geometric morphometric analysis of skull shape. Evol Dev 13:204–213

Emerson SB, Bramble DM (1993) Scaling, allometry and skull design. In: Hanken J, Hall BK (eds) The skull. The University of Chicago Press, Chicago, pp 384–416

Evans HE (1993) Miller's anatomy of the dog, 3rd edn. W.B. Saunders Company, Philadelphia
Ewer R (1973) The carnivores. Cornell University Press, Ithaca
Finarelli JA, Goswami A (2009) The evolution of orbit orientation and encephalization in the carnivora (Mammalia). J Anat 214:671–678
Flores DA, Giannini NP, Abdala F (2003) Cranial ontogeny on *Lutreolina crassicaudata* (Didelphidae): a comparison with *Didelphis albiventris*. Acta Theriol 48:1–9
Flores DA, Giannini NP, Abdala F (2006) Comparative postnatal ontogeny of the skull in an Australidelphian Metatherian, *Dasyurus albopunctatus* (Marsupialia: Dasyuromorpha: Dasyuridae). J Morphol 267:426–440
Flores DA, Giannini NP, Abdala F (2010) Cranial ontogeny of *Caluromys philander* (Didelphidae: Caluromyinae): a qualitative and quantitative approach. J Mamm 91:539–550
Fox MW (1964) The ontogeny of behaviour and neurologic responses in the dog. Ani Behav 12:301–310
Fox MW (1969) Ontogeny of prey-killing behavior in Canidae. Behaviour 35:259–272
Gay SW, Best TL (1996) Age-related variation in skulls of the puma (*Puma concolor*). J Mamm 77:191–198
Giannini NP, Abdala F, Flores DA (2004) Comparative postnatal ontogeny of the skull in *Dromiciops gliroides* (Marsupialia: Microbiotheriidae). Am Mus Novit 3460:1–17
Giannini NP, Segura V, Giannini MI, Flores D (2010) A quantitative approach to the cranial ontogeny of the puma. Mamm Biol 75:547–554
Goodall C (1991) Procrustes methods in the statistical analysis of shape. J R Stat Soc 53:285–339
Hammer Ø, Harper DAT, Ryan PD (2001) PAST: paleontological statistics software package for education and data analysis. Palaeontol Electronica 4:1–9. http://palaeo-electronica.org/2001_1/past/past.pdf. Accessed 28 February 2011
Holekamp KE, Kolowski JM (2009) Family Hyaenidae (Hyenas). In: Wilson DE, Mittermeier RA (eds) Handbook of the mammals of the world 1 carnivores. Lynx Editions, Barcelona, pp 234–260
Jiménez JE, Novaro AJ (2004) *Pseudalopex culpaeus* (Molina, 1782). In: Sillero-Zubiri C, Hoffmann M, Macdonald DW (eds) Canids: foxes, wolves, jackals and dogs. Status Survey and Conservation Action Plan, IUCN/SSC Canid Specialist Group, Gland, pp 44–49
Johnson WE, Franklin WL (1994) Role of body size in the diets of sympatric gray and culpeo foxes. J Mamm 75:163–174
Jolicoeur P (1963a) The multivariate generalization of the allometry equation. Biometrics 19:497–499
Jolicoeur P (1963b) The degree of generality of robustness in *Martes americana*. Growth 27:1–27
Kraglievich L (1930) Craneometría y clasificación de los cánidos sudamericanos, especialmente los argentinos actuales y fósiles. Physis 10:35–73
Kremenak CR (1969) Dental eruption chronology in dogs: deciduous tooth gingival emergence. J Dent Res 48:1177–1184
Kremenak CR, Russell LS, Christensen RD (1969) Tooth-eruption ages in suckling dogs as affected by local heating. J Dent Res 48:427–430
La Croix S, Holekamp KE, Shivik JA, Lundrigan BL, Zelditch ML (2011) Ontogenetic relationships between cranium and mandible in coyotes and hyenas. J Morphol 272:662–674
Manly BFJ (1997) Randomization, bootstrap, and Monte Carlo methods in biology. Chapman & Hall, New York
Moore WJ (1981) The mammalian skull. Cambridge University Press, UK
Noble VE, Kowalski EM, Ravosa MJ (2000) Orbit orientation and the function of the mammalian postorbital bar. J Zool 250:405–418
Novaro AJ (1997) *Pseudalopex culpaeus*. Mamm Species 558:1–8
Prevosti FJ, Lamas L (2006) Variation of cranial and dental measurements and dental correlations in the pampean fox *Dusicyon gymnocercus*. J Zool 270:636–649
Radinsky LB (1981) Evolution of skull shape in carnivores. I. Representative modern carnivores. Biol J Linn Soc 15:369–388
Ravosa MJ, Noble V, Hylander W, Johnson K, Kowalski E (2000) Masticatory stress, orbital orientation and the evolution of the primate postorbital bar. J Hum Evol 38:667–693
Rohlf FJ (1999) Shape statistics: procrustes method for the optimal superimposition of landmarks. Syst Zool 39:40–59
Rohlf FJ (2003a) TpsRegr version 1.28. Department of Ecology and Evolution, State University of New York at Stony Brook, Stony Brook. http://life.bio.sunysb.edu/morph/. Accessed 2 March 2011
Rohlf FJ (2003b) TpsRelw version 1.35. Department of Ecology and Evolution, State University of New York at Stony Brook, Stony Brook. http://life.bio.sunysb.edu/morph/. Accessed 2 March 2011
Rohlf FJ (2008a) TpsUtil version 1.40. Department of Ecology and Evolution, State University of New York at Stony Brook, Stony Brook. http://life.bio.sunysb.edu/morph/. Accessed 2 March 2011
Rohlf FJ (2008b) TpsDig version 2.12. Department of Ecology and Evolution, State University of New York at Stony Brook, Stony Brook. http://life.bio.sunysb.edu/morph/. Accessed 2 March 2011
Scott JP (1967) The evolution of social behavior in dogs and wolves. Am Zool 7:373–381
Segura V, Flores D (2009) Aproximación cualitativa y aspectos funcionales en la ontogenia craneana de *Puma concolor* (felidae). Mastozool Neotrop 16:169–182
Sheets HD (2002) IMP-integrated morphometrics package. Department of Physics, Casius College, Buffalo
Slater GJ, Dumont E, Van Valkenburgh B (2009) Implications of predatory specialization for cranial form and function in canids. J Zool 278:181–188
Tanner JB, Zelditch ML, Lundrigan BL, Holekamp KE (2010) Ontogenetic change in skull morphology and mechanical advantage in the spotted hyena (*Crocuta crocuta*). J Morphol 271:353–365
R Development Core Team (2004) R: a language and environment for statistical computing. R Foundation for Statistical Computing, Vienna. http://www.rproject.org. Accessed 26 Feb 2011
Travaini A, Juste J, Novaro A, Capurro A (2000) Sexual dimorphism and sex identification in the South American culpeo fox, *Pseudalopex culpaeus* (Carnivora: Canidae). Wildlife Res 27:669–674
Tseng ZJ (2009) Cranial function in a late Miocene *Dinocrocuta gigantea* (Mammalia: Carnivora) revealed by comparative finite element analysis. Biol J Linn Soc 96:51–67
Tseng ZJ, Binder WJ (2010) Mandibular biomechanics of *Crocuta crocuta*, *Canis lupus*, and the late Miocene *Dinocrocuta gigantea* (Carnivora, Mammalia). Zool J Linn Soc 158:683–696
Tseng ZJ, Wang X (2010) Cranial functional morphology of fossil dogs and adaptation for durophagy in *Borophagus* and *Epicyon* (Carnivora, Mammalia). J Morphol 271:1386–1398
Tukey JW (1956) Bias and confidence in not quite large samples. Ann Math Stat 23:614
Van Valkenburgh B (1988) Trophic diversity in past and present guilds of large predatory mammals. Paleobiology 14:155–173
Van Valkenburgh B (1989) Carnivore dental adaptations and diet: a study of trophic diversity within guilds. In: Gittleman JL (ed) Carnivore behavior, ecology, and evolution. Cornell University Press, Ithaca, pp 410–436
Van Valkenburgh B (2007) Déjà vu: the evolution of feeding morphologies in the carnivora. Integr Comp Biol 47:147–163
Van Valkenburgh B, Koepfli KP (1993) Cranial and dental adaptations to predation in canids. Symp Zool Soc Lond 65:15–37
Wayne RK (1986) Cranial morphology of domestic and wild canids: the influence of development on morphological change. Evolution 40:243–261

Zapata SC, Funes M, Novaro A (1997) Estimación de la edad en el zorro colorado patagónico (*Pseudalopex culpaeus*). Mastozool Neotrop 4:145–150

Zar JH (1984) Biostatistical analysis. Prentice-Hall Inc, Englewood Cliff

Zelditch ML, Swiderski D, Sheets H, Fink W (2004) Geometric morphometrics for biologists: a primer. Elsevier Academic Press, London